REPORT DOCUMENTATION PAGE

Form Approved
OMB No. 0704-0188

1. AGENCY USE ONLY *(Leave blank)*	2. REPORT DATE	3. REPORT TYPE AND DATES COVERED
	November 1992	Technical Paper

4. TITLE AND SUBTITLE
An Approach to Constrained Aerodynamic Design With Application to Airfoils

5. FUNDING NUMBERS
WU 505-59-10-03

6. AUTHOR(S)
Richard L. Campbell

7. PERFORMING ORGANIZATION NAME(S) AND ADDRESS(ES)
NASA Langley Research Center
Hampton, VA 23681-0001

8. PERFORMING ORGANIZATION REPORT NUMBER
L-17108

9. SPONSORING/MONITORING AGENCY NAME(S) AND ADDRESS(ES)
National Aeronautics and Space Administration
Washington, DC 20546-0001

10. SPONSORING/MONITORING AGENCY REPORT NUMBER
NASA TP-3260

11. SUPPLEMENTARY NOTES

12a. DISTRIBUTION/AVAILABILITY STATEMENT
Unclassified–Unlimited

Subject Category 02

12b. DISTRIBUTION CODE

13. ABSTRACT *(Maximum 200 words)*

An approach has been developed for incorporating flow and geometric constraints into the Direct Iterative Surface Curvature (DISC) design method. In this approach, an initial target pressure distribution is developed using a set of control points. The chordwise locations and pressure levels of these points are initially estimated either from empirical relationships and observed characteristics of pressure distributions for a given class of airfoils or by fitting the points to an existing pressure distribution. These values are then automatically adjusted during the design process to satisfy the flow and geometric constraints. The flow constraints currently available are lift, wave drag, pitching moment, pressure gradient, and local pressure levels. The geometric constraint options include maximum thickness, local thickness, leading-edge radius, and a "glove" constraint involving inner and outer bounding surfaces. This design method has also been extended to include the successive constraint release (SCR) approach to constrained minimization.

14. SUBJECT TERMS
Airfoil design; Design method

15. NUMBER OF PAGES
22

16. PRICE CODE
A03

17. SECURITY CLASSIFICATION OF REPORT	18. SECURITY CLASSIFICATION OF THIS PAGE	19. SECURITY CLASSIFICATION OF ABSTRACT	20. LIMITATION OF ABSTRACT
Unclassified	Unclassified		

Summary

An approach has been developed for incorporating flow and geometric constraints into the Direct Iterative Surface Curvature (DISC) design method. In this approach, an initial target pressure distribution is developed using a set of control points. The chordwise locations and pressure levels of these points are initially estimated either from empirical relationships and observed characteristics of pressure distributions for a given class of airfoils or by fitting the points to an existing pressure distribution. These values are then automatically adjusted during the design process to satisfy the flow and geometric constraints. The flow constraints currently available are lift, wave drag, pitching moment, pressure gradient, and local pressure levels. The geometric constraint options include maximum thickness, local thickness, leading-edge radius, and a "glove" constraint involving inner and outer bounding surfaces. This design method has also been extended to include the successive constraint release (SCR) approach to constrained minimization.

A number of test cases have been included to illustrate the two automated approaches to generating the initial target pressures as well as to demonstrate the various constraint options. Unconstrained design results using just the initial target distributions indicate that the automated target generation procedures can yield airfoils that have flow and geometric parameters that are fairly close to the desired values. Invoking the constrained design capability then provides a very close match to these target values in general. Because of a good initial target distribution and the use of a simultaneous flow, design, and target convergence approach, a constrained design requires about the same amount of computer time as a design using just the basic DISC method. Although the DISC design method was used for the cases in this study, the target generation and modification procedures can be used with any design method that uses a specified pressure distribution as its objective.

Introduction

In the last few years, advanced Computational Fluid Dynamics (CFD) analysis methods have begun shifting from the domain of code development to the arena of applied aerodynamics. Both Euler and Navier-Stokes codes are being used routinely in the design and analysis of configurations ranging from airfoils to complete aircraft. Although their use is still somewhat limited because of the large computer resource requirement, the continued progress in both algorithm efficiency and computer speed will soon make them a viable option for many research and design applications.

A natural extension of these analysis capabilities is the development of related automated design methods. These design methods may be divided into two general categories: (1) methods that employ an inverse solver in at least part of the computational domain, and (2) methods that utilize direct analyses in an iterative manner. Classical inverse codes, such as those of Giles and Drela (1986) and Volpe and Melnik (1985), and the fictitious-gas method of Sobieczky et al. (1979) are examples of the first category. Numerical optimization (Hicks, Murman, and Vanderplaats 1974) and the Direct Iterative Surface Curvature (DISC) method of Campbell and Smith (1987a, 1987b) fall into the second category. These direct approaches can be coupled with any analysis method and thus take advantage of the experience and confidence levels already established for the chosen code. Since they are also relatively easy to couple with existing analysis codes, a designer can utilize the latest computational technology. Good overviews as well as many individual examples of the state of the art of automated design methods are given in Anon. (1990a) and in Anon. (1990b).

As noted by Dulikravich (1990), the design problem most often addressed by automated design methods is that of obtaining the geometry that will yield a specified surface pressure or velocity distribution. Two exceptions to this are the fictitious-gas method and the optimization to a global objective function such as drag. In the fictitious-gas approach, a shock-free supercritical flow is obtained; however, no direct control is available over either the surface pressures or geometry. The use of a global objective function in optimization (to minimize wave drag, for example) is attractive in that it deals directly with the parameters of interest for design. Unfortunately, the global parameter most often used (drag) is also the one that is generally the least accurately calculated and is slow to converge. This means that long run times may be required to get sufficiently accurate sensitivity derivatives for use in the optimizing routines. Also, the results obtained are very dependent on the shape functions used as design variables, and problems with uniqueness and unrealistically high pressure gradients in some regions have been reported (Van den Dam, Van Egmond, and Slooff 1990). These difficulties are largely alleviated by specifying the surface pressures, although problems such as "hanging" shocks and physically unrealistic airfoils may still occur unless appropriate constraints are enforced (Volpe and Melnik 1985).

In developing an airfoil or wing, consideration must be given not only to the aerodynamic characteristics that yield good performance, stability, and control but also to the geometric constraints arising from structural or manufacturing considerations as well as from overall design requirements such as fuel volume. For the inverse design problem where surface pressures are specified, the main task thus becomes that of defining a "good" target pressure distribution, that is, one that satisfies both the flow and geometric objectives and constraints. Generating a target pressure distribution that has a given lift and pitching moment is straightforward, since these quantities are closely approximated by simple integrations of the pressures over the chord. Also, reasonable estimates of the drag levels may be obtained from approximations for the wave, skin friction, and induced-drag components. Although it is not a trivial task, a target pressure distribution that satisfies all these flow requirements can be determined, usually by trial and error. (A more interesting approach is the use of numerical optimization to generate a target pressure distribution (Van Egmond 1990).) The difficulty that then arises, however, is that the geometric characteristics corresponding to this pressure distribution are not known prior to the design, thus resulting in the need to alter the target pressures to match both the flow and geometric constraints. These modifications to the target pressures are also usually not automated, and even with a good knowledge of pressure-geometry relationships, the modifications often require a number of attempts before a satisfactory target distribution is achieved.

An approach to constrained aerodynamic design is presented in this report. With this approach, the initial target pressures are automatically generated and subsequently modified to meet global and local flow constraints (such as lift, wave drag, and local pressure gradients) as well as geometric requirements (such as maximum or local thickness). A method for systematically releasing some of these constraints in order to minimize an objective function is also described. This method has many of the advantages of classical numerical optimization using global parameters, but it is much less time intensive and thus less expensive than optimization. Although the DISC design method was used in this study to illustrate the constrained design approach, the technique should be applicable to any design method that uses a given target pressure distribution as its objective. After a brief review of the basic DISC design method, a description of the constrained design approach is given, which is followed by a discussion of the minimization technique. In each section, airfoil design examples are included to illustrate the capabilities of the methods.

Symbols

C	surface curvature, nondimensionalized by chord
C_{le}	nondimensional surface curvature at leading edge
C_p	pressure coefficient
C_p^*	sonic pressure coefficient
$C_{p,o}$	stagnation pressure coefficient
c	local chord
$c_{d,w}$	section wave-drag coefficient
$\tilde{c}_d$	composite drag objective function
c_l	section lift coefficient
c_m	section pitching-moment coefficient
J	grid-point index in normal direction
J_s	grid-point index to begin perturbation decay
M	local Mach number
M_1	shock Mach number
M_∞	free-stream Mach number
N	outermost grid-point index in normal direction
r_{le}	leading-edge radius, nondimensionalized by chord
t	thickness
t/c	maximum airfoil thickness-chord ratio
X, x	streamwise coordinates
Y, y	vertical coordinates
Abbreviations:	
L.S.	lower surface
U.S.	upper surface

Basic DISC Design Method

The basic DISC design method consists of two components: a flow solver and the DISC design module. The specific flow analysis code chosen for this study is described in the next section. The subsequent section contains a discussion of the DISC

design module and how it is coupled to the analysis code.

Flow Solver

The flow solver selected for use in this study is a code developed by Hartwich (1990). This code (later named the GAUSS2 code) uses a fast implicit upwind procedure to solve the two-dimensional, nonconservative Euler equations on a structured mesh. The meshes used in this study were 161 by 33 C-type grids developed using a separate grid-generation code. A floating shock-fitting approach is employed that gives sharply defined shocks even on coarse grids. In regions away from a shock, a second-order, split-coefficient-matrix upwinding method is used. Convergence to steady state is accelerated by a diagonalized approximate factorization technique.

Viscous effects have been incorporated into the code using a boundary-layer displacement-thickness approach. Two boundary-layer options are available: the Nash and Macdonald (1967) method, and a modified version of the approach of Stratford and Beavers (1961). The second option is not quite as accurate as the Nash method, but it is far more stable for flows with small regions of separation. For both approaches, the viscous drag is estimated using the Squire-Young (1938) technique.

For the results in this study, the lift and pitching-moment coefficients were obtained by pressure integration. The total drag coefficient was determined by adding the viscous drag component from the boundary-layer calculation to a wave-drag coefficient computed using the far-field entropy-based approach derived by Oswatitsch (1956). The GAUSS2 code is especially well suited to this form of wave-drag computation since one of the dependent variables in the flow solver is entropy which, because of the shock-fitting approach, is generated only at shocks. The airfoil design code developed by coupling this flow solver with the DISC design module described in the next section is referred to as the DGAUSS code.

DISC Design Module

The basic DISC design method is an iterative procedure that links the design module with a CFD analysis code to modify an initial aerodynamic surface geometry so that it produces a specified pressure distribution. A flowchart illustrating this method is given in figure 1. The process begins by analyzing the initial geometry at the design conditions in the flow code to obtain the surface pressure distribution. The current pressures are then compared with the target pressure distribution in the design module, and the surface geometry is modified using a hybrid design algorithm that depends on the local Mach number.

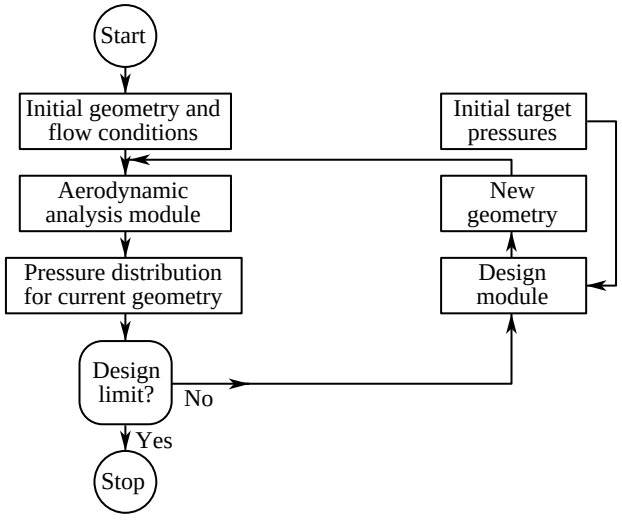

Figure 1. Flowchart of basic DISC design method.

For subsonic and low-supersonic Mach numbers ($M \leq 1.1$), the required change in surface curvature (ΔC) is related to the difference between target and analysis pressure coefficients (ΔC_p) by the equation

$$\Delta C = \Delta C_p \; A(1 + C^2)^B \tag{1}$$

where A is a relaxation factor that is positive for the upper surface and negative for the lower surface. The exponent B may vary between 0 and 0.5 (a typical value is 0.2), with higher values yielding faster design convergence but less stability in the nose region of an airfoil. When the local Mach number is above 1.1, the equation initially used is

$$\Delta C = \frac{d(\Delta C_p)}{dx} \; \frac{A\sqrt{M_\infty^2 - 1}}{2} \; \frac{1}{[1 + (dy/dx)^2]^{1.5}} \tag{2}$$

When the streamwise slopes of the analysis pressures are close to the corresponding slopes of the target distribution, equation (1) is used in combination with equation (2) to adjust the analysis pressure levels more quickly. Since equation (2) is not technically valid when the free-stream Mach number is less than 1.0, an effective free-stream Mach number of 1.01 is used for the subsonic cases. Detailed derivations of these design algorithms are given by Campbell and Smith (1987a, 1987b) and Smith and Campbell (1991).

These equations are applied at each point I along both airfoil surfaces, marching from the leading edge to the trailing edge. The local curvature changes are made by shearing the points aft of the current one

through a given angle. (See fig. 2(a).) This approach results in minimal changes to the curvatures at the other points; however, at the end of the design sweep, the airfoil will typically have either an open or crossed trailing edge. To remedy this situation, the surface is rotated about the leading edge back to the original trailing-edge location (fig. 2(b).) Smoothing is applied to both the airfoil surface and the nose camber line to ensure that a reasonable airfoil geometry is maintained throughout the design process. The smoothing technique is based on a least-squares fit of a polynomial curve through the surface or camber line coordinates and is described in Smith and Campbell (1991).

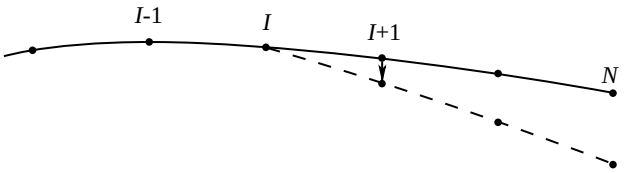

(a) Shear surface segment to change curvature at a point.

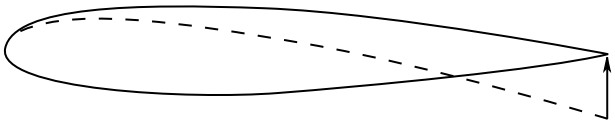

(b) Rotate entire surface to recover original trailing-edge points.

Figure 2. Procedure for modifying airfoil geometry.

Once a new surface is obtained, a grid must be developed that incorporates the modified geometry. Although a few codes have an internal grid-generation capability that can be used for this task, the majority of the advanced CFD codes require the grid to be supplied from an external source. A simple method to modify the original grid has been developed and incorporated into the basic DISC design module. In this approach (see fig. 3), the perturbation at a surface grid point is added in a linearly decaying fashion to each successive point along a grid line that is normal to the airfoil surface, with the result that the grid points at the outer boundary of the grid block remain unchanged. This method works well for Euler grids that have a fairly coarse spacing between points in the normal direction. For the highly stretched Navier-Stokes grids with many points near the surface, the method was modified to keep a constant perturbation for the grid points near the surface and to begin the linear decay at some point (J_s) away from the surface. This point is typically selected to include the inner third of the grid points, but it may include the entire field grid if the outer boundary does not need to stay fixed. To maintain grid quality, an additional routine was developed to reestablish grid orthogonality in the vicinity of the airfoil surface.

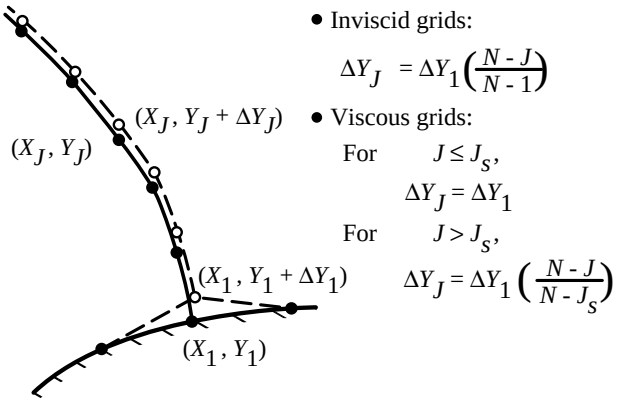

Figure 3. Grid perturbation approaches.

Although an airfoil has been used in this description of the DISC design method, the basic approach is applicable to any external aerodynamic surface having primarily attached flow. Three-dimensional surfaces may be designed by applying the method to sections of a component in a strip fashion. Even though a section is not restricted to be planar, it must be approximately aligned with the local flow direction. A number of examples of wing design using this approach are given by Campbell and Smith (1987a, 1987b) and Smith and Campbell (1991). Other aircraft components that have been designed using this method include winglets (Lin, Chen, and Tinoco 1990) and nacelles ((Lin, Chen, and Tinoco 1990), (Wie, Collier, and Wagner 1991), and (Bell, and Cedar 1991)). For applications involving internal flow, including flow channeling between aircraft components, the method would have to be modified to account for changes in channel area.

Constrained Design Approach

Even though the aerodynamic design process is primarily focused on the aerodynamic characteristics that relate to the performance of an aircraft (such as lift, drag, or pitching moment), the requirements imposed by other disciplines must also be taken into account. These requirements can often be translated into geometric constraints such as airfoil thicknesses at certain locations for structural strength or wing volume for fuel.

In the basic DISC design approach, the aerodynamic constraints are addressed by the formulation

of the inverse design problem. Once a target pressure distribution over the chord of an airfoil has been specified, the lift and pitching-moment coefficients may be determined with sufficient accuracy by simple integration if the angle of attack is small. The drag coefficient cannot be determined *a priori* from pressure integration since the airfoil ordinates are not known. However, this pressure integration method of determining the drag coefficient is often not very accurate, and other approaches for calculating the total drag or various components of the drag are often used. Some of these methods can be used to obtain a good approximation of the drag without knowing the details of the airfoil geometry. (These will be discussed in a subsequent section of this paper.)

A target pressure distribution can thus be generated that will match the aerodynamic design objectives. However, this distribution is not unique; many different distributions can be developed that will satisfy these design constraints, each of which will have a unique geometry associated with it. These airfoil shapes may or may not meet the geometric constraints imposed by the other disciplines. The design task is then to obtain a target pressure distribution that will simultaneously satisfy both the aerodynamic and geometric design constraints.

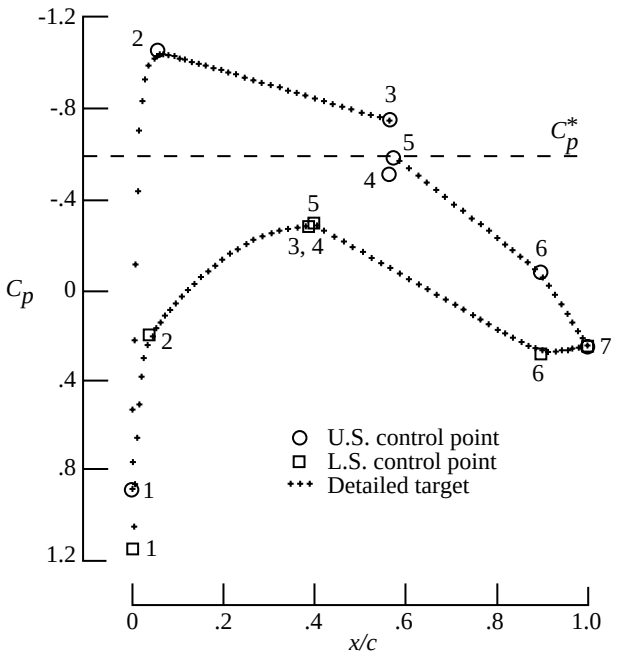

Figure 4. Control points used to develop target pressure distribution.

A procedure has been developed that will automatically perform this task. This procedure includes (1) two approaches for generating initial target pressure distributions based on the aerodynamic and geometric constraints, and (2) a method for iteratively modifying the target pressures during the design process. In order to manipulate the detailed target pressures during both the generation and modification phases, the pressure distribution is divided into regions bounded by control points, as shown in figure 4. This procedure is similar to that used by Malone, Narramore, and Sankar (1990) and Van Egmond (1990) in that the locations of the control points are determined, in general, by the flow characteristics. The philosophy used in the current procedure to locate each control point is described below.

Unless specifically noted, the locations of the corresponding points on the upper and lower surfaces are determined in the same manner. Point 1 on each surface corresponds to the leading edge, or to the stagnation point location if it is aft of the leading edge. This is followed by a leading-edge acceleration region that ends at point 2. The segment between points 2 and 3 is usually a region of fairly mild pressure gradients, especially at cruise design conditions. For example, this would correspond to the flat rooftop region on a supercritical airfoil. Point 4 is used to represent the jump in pressure across a shock when a shock is present; otherwise, point 4 is coincident with point 3. The location of point 5 is selected to correspond approximately with the location of the maximum airfoil thickness (instead of being based on a flow criterion). Currently, point 5 is restricted to being aft of the shock location (point 4). Although the actual location of maximum airfoil thickness may be ahead of this point, it is usually close enough for the changes in pressure level at point 5 to have the desired effect on the airfoil thickness. Point 6 is placed between the maximum-thickness control point and the trailing edge (point 7) according to the following criteria. For airfoils with little aft camber, the location of point 6 corresponds with the beginning of the final pressure recovery region on both the upper and lower surfaces. For supercritical airfoils with high aft camber, point 6 is placed at the maximum pressure coefficient in the cove region on the lower surface, and also near the beginning of the main recovery gradient on the upper surface.

Target Pressure Generation

As mentioned in the previous section, the goal of the procedure for automated target pressure generation is to define an initial detailed target distribution for use in the DISC method by using just the aerodynamic and geometric constraints as input. In

order to accomplish this, the procedure must not only be able to determine the chordwise location and pressure level associated with each control point but must also be able to describe the shape of the pressure distribution between the control points. Approaches for accomplishing both of these tasks are described below.

Two approaches for determining the control point values have been implemented. In the first approach, the initial values are determined from empirical pressure-geometry relationships and characteristics observed for existing airfoils. The second approach involves fitting the control points to an existing pressure distribution, often generated by analyzing the airfoil to be modified. For both approaches, several initial pressure levels are systematically adjusted to meet the flow constraints while maintaining the pressure levels associated with the geometric constraints. The details of these two approaches, along with examples that illustrate the techniques, are given in the following sections. Thus far, these approaches have been applied only to airfoils at moderate lift coefficients and subsonic freestream Mach numbers. In principle, however, the approaches should be valid for high lift or supersonic flows as long as the flow is attached and the pressure-geometry relationships used are developed from similar flows.

Empirical Estimation Approach

In the empirical estimation approach, the initial locations and pressure levels of the control points are, in general, determined from empirically derived equations with global flow and geometric parameters as the independent variables. The specific formulas for each point used in this paper are given below. One should note that these formulas are not rigorously derived but are developed either by curve fitting experimental data or by modifying simple analytical relationships. The intent of this section is not to prescribe the best pressure-geometry relationships available but to illustrate that this approach for defining target pressures can produce good results, even when fairly crude approximations for the relationships between the target pressures and the flow and geometric parameters are used. To simplify the equations for these relationships in the following sections, a chord of 1.0 is assumed, with the result that x/c becomes x.

Determination of control point locations and levels. The formulas for the locations and levels of the first control point on each surface are empirically defined from studies of experimental data and CFD results. For airfoils at cruise conditions, the stagnation point is generally very close to the leading edge on the lower surface. Thus, the location of the first control point on the lower surface is obtained from the following estimate for the location of the stagnation point at lifting conditions:

$$(x_1)_{\text{lower}} = 0.01(c_l + 4c_m)\sqrt{1 - M_\infty^2} \tag{3}$$

with the corresponding pressure coefficient estimated from

$$(C_{p,1})_{\text{lower}} = C_{p,o} \approx 1 + 0.27M_\infty^2 \tag{4}$$

which is an approximation to the isentropic stagnation pressure relationship. The location of point 1 on the upper surface is set to $x = 0$, and the pressure coefficient is specified by

$$(C_{p,1})_{\text{upper}} = C_{p,o} - (c_l + 4c_m)\frac{0.015}{r_{le}} \tag{5}$$

The chordwise locations of the second control points are used in meeting the leading-edge-radius constraint. For airfoils with the stagnation point at the leading edge, a steeper acceleration region (i.e., control point 2 farther forward for a given C_p level) will give a blunter airfoil, whereas a milder pressure gradient between points 1 and 2 will tend to reduce the nose radius. The initial location of control point 2 on the upper surface is defined by using the empirical relation

$$x_2 = 0.5t/c \tag{6}$$

For the lower surface, this value is reduced by 0.02 to account for the fact that, in general, less acceleration is required to meet the lower surface pressure levels.

The initial values for the pressure coefficients at points 2 and 3 are determined by using both the lift coefficient and the thickness constraint. The equation used to compute these initial values is

$$C_{p,2} \text{ or } C_{p,3} = C_{p,t} \pm C_{p,l} \tag{7}$$

where $C_{p,t}$ is the contribution due to airfoil thickness and is given by

$$C_{p,t} = \frac{At/c}{\sqrt{1 - M_\infty^2}} \tag{8}$$

and $C_{p,l}$ is given by

$$C_{p,l} = -0.5c_l \tag{9}$$

to provide an initial uniform chordwise distribution of lift. Based on computational results for airfoils, the coefficient A in equation (8) was assigned a value of -3.3. In equation (7), the positive and

negative signs are used for the upper and lower surfaces, respectively. Increasing the magnitude of $C_{p,l}$ will tend to increase the amount of camber in the midchord region for a constant airfoil incidence.

The third control point on each surface is initially located at $x = 0.4$. When a shock is present, this point is moved to

$$x_3 = M_\infty^2 \tag{10}$$

based on observations of pressure distributions for current supercritical airfoils at transonic speeds. This location represents a nominal value with actual shock locations varying by about $\pm 0.1c$ from this value, depending on the airfoil thickness and lift coefficient.

For cases involving supercritical flow, control point 3 represents the termination of the initial supersonic flow region and is affected by the wave-drag constraint. This constraint is implemented by relating the wave-drag coefficient to the pressure level just ahead of the shock. Lock (1985) derives an expression for estimating the wave drag from the free-stream Mach number, the shock Mach number M_1, and the surface curvature at the shock. Unfortunately, this formula cannot be used for generating the initial target pressures since the local surface curvatures are not known until the design is completed. A similar equation has therefore been empirically developed using results from the GAUSS2 code for several airfoils from the NACA 4-digit series, and this equation is given as

$$c_{d,w} = A_1(M_1 - 1)^4 \tag{11}$$

where the coefficient A_1 is given by

$$A_1 = \frac{0.04}{(t/c)^{1.5}} \tag{12}$$

With this approach, the surface curvature at the shock location has been implicitly accounted for by the global parameter t/c. In figure 5, the wave-drag coefficients estimated from equation (11) are compared with the values computed by the GAUSS2 code. The correlation is good in general, especially for the larger values of thickness that would correspond to subsonic transport airfoils. By specifying a desired wave-drag coefficient and maximum airfoil thickness, the maximum allowable shock Mach number can be determined. This value is then converted to a minimum pressure-coefficient constraint imposed at point 3 on the upper surface. To improve the accuracy of equation (11), the coefficient A_1 can be recalibrated during a design run to reflect the current values of $c_{d,w}$ and M_1.

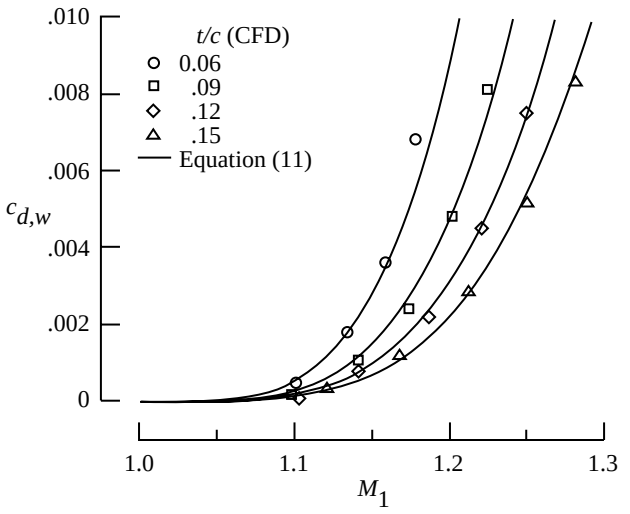

Figure 5. Correlation between empirical and CFD wave-drag coefficients for NACA 4-digit series airfoils.

Control point 4 is coincident with point 3 for subcritical flow. For supercritical flow, the pressure coefficient at point 4 is computed using the Rankine-Hugoniot equation with an empirical modification that reduces the shock jump and more accurately matches results from the GAUSS2 code as well as experimental values. The maximum-thickness control point (point 5) is located $0.01c$ aft of point 4. The pressure coefficient is calculated using equation (7) with the restriction that the value cannot be more negative than the sonic pressure coefficient.

Control point 7 is located at the trailing edge with a pressure coefficient given by

$$C_{p,7} = 2t/c \tag{13}$$

The values for control point 6 are determined by different methods, depending on the specified value of the pitching moment. The chordwise locations of the upper and lower surface points are initially set to $x = 0.9$. For aft-loaded airfoils ($c_m \leq -0.1$), the upper surface point is moved to midway between point 5 and point 7 at the trailing edge. The pressure coefficient is computed using an equation similar to equation (7), with a thickness and a lift component. For both types of airfoils, the thickness part is given by the nonlinear interpolation formula

$$C_{p,t,6} = C_{p,t} + (C_{p,7} - C_{p,t})\frac{\bar{x}_6 - x_5}{(x_7 - x_5)^{0.7}} \tag{14}$$

where $\bar{x}_6$ is the average of the locations of the upper and lower control points and $C_{p,t}$ is the value from

equation (8). The lift component at point 6 is computed using linear interpolation from

$$C_{p,l,6} = C_{p,l} \frac{x_7 - \bar{x}_6}{x_7 - x_5} \tag{15}$$

where $C_{p,l}$ is determined from equation (9).

Generation of detailed target pressure distribution. Once the initial control point values are selected, a detailed target distribution is developed by first connecting the control points with simple analytic functions and then computing the pressure levels at points corresponding to the initial airfoil surface grid. These functions can be specified to match the general shape of pressure distributions for different classes of airfoils and different design conditions (e.g., cruise condition versus low-speed, high-lift condition). The functions are typically either straight lines or parabolas except at the leading edge where fourth-order and third-order polynomials are used for the upper and lower surfaces, respectively. When the first control point on the lower surface is aft of the leading edge, a linear segment is placed between the first control point on the upper surface (leading edge) and the first one on the lower surface (stagnation point). The values near the control points are smoothed using a three-point, weighted, linear averaging technique to reduce any slope discontinuities that may occur at segment junctions.

Integrating this detailed target pressure distribution will yield lift and pitching-moment coefficients. If the value of $C_{p,l}$ from equation (9) is applied to all the control points, this lift coefficient will match the desired lift coefficient exactly. Since this is not the case for the leading- and trailing-edge pressures, where the respective upper and lower surface pressures are identical, the resulting lift is less than the constraint value. Also, since the desired value of pitching moment is not used in any expressions that determine pressure levels, satisfying the pitching-moment constraint would only be fortuitous. The pressure levels of control points 2 and 6 are therefore iteratively adjusted so that both the lift and pitching-moment constraints are met. In order to maintain reasonable pressure gradients between control points 2 and 3 on each surface, a minimum pressure coefficient level is established for point 2 on the upper surface and a maximum level is set for point 2 on the lower surface. An additional constraint is that the pressure coefficient at point 6 on the upper surface should be less than the corresponding value on the lower surface. Because of these restrictions, the problem is possibly overconstrained and the iteration on the lift and pitching moment will not converge to the required values. Since the lift coefficient is typically an inflexible requirement, a mechanism has been included to release either the pitching-moment or the wave-drag constraint until the target lift coefficient can be matched. This mechanism is the basis of the minimization approach that is discussed in a later section of this report.

Example using the empirical estimation approach. A target pressure distribution has been generated for a supercritical airfoil at a transonic cruise design point to illustrate the empirical estimation approach. The flow constraints for this case are a free-stream Mach number of 0.75, a lift coefficient of 0.6, a wave-drag coefficient less than or equal to 0.0005, and a pitching-moment coefficient no more negative than -0.15. The geometric constraints include a maximum thickness-chord ratio of 0.120 and a leading-edge radius of $0.016c$. The latter value was obtained from the desired thickness and the radius-thickness relationship for the NACA 4-digit airfoil series. Note that both two-sided (equality) and one-sided (inequality) constraints are specified and can be used for any variables in this case.

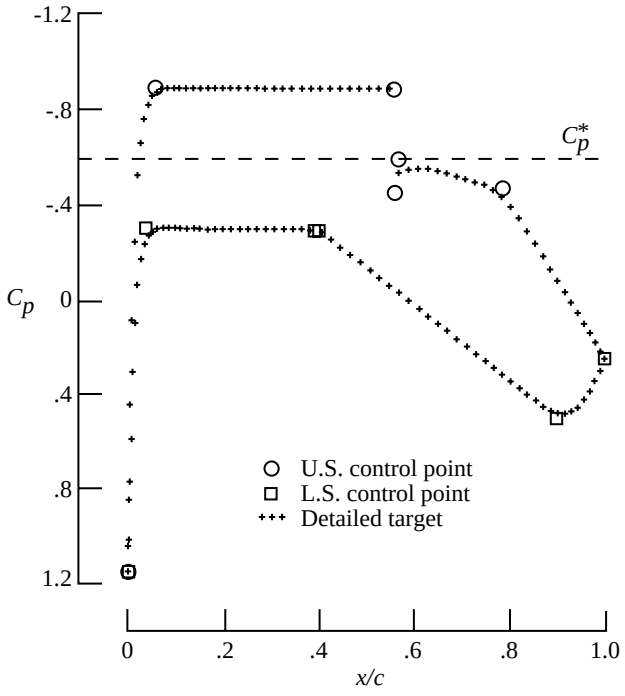

Figure 6. Control points and detailed target pressures from empirical estimation approach for $M_\infty = 0.75$ and $c_l = 0.6$.

The control points and the associated detailed target distribution developed using the above constraints are shown in figure 6. The distribution has the flat supersonic rooftop and aft loading typical of

supercritical airfoils. The detailed target does not exactly match the control points because of the smoothing applied at the segment junctures.

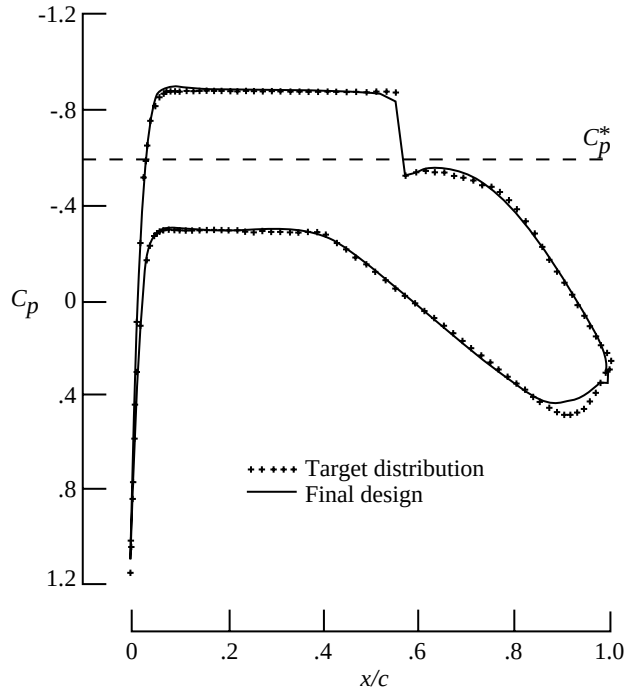

(a) Pressure distribution.

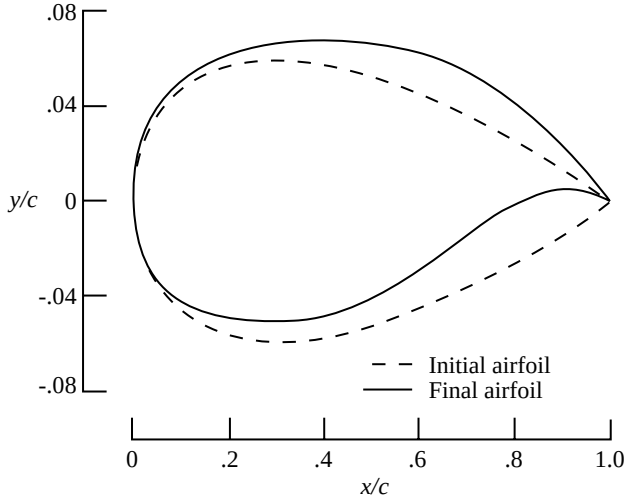

(b) Airfoil.

Figure 7. Basic DISC design results from empirical estimation approach for $M_\infty = 0.75$ and $c_l = 0.6$.

An airfoil was developed from this target using the DGAUSS code in the basic DISC design mode. An NACA 0012 airfoil was used to start the design process at an angle of attack of 0°. Although no design constraints relative to viscous drag are currently available, the modified Stratford boundary-layer computation was included in the flow solver module with the Reynolds number set to 10×10^6 based on the airfoil chord. The pressures from the final design cycle are compared with the target distribution in figure 7(a). The design pressures match the target values fairly well except near the trailing edge on the lower surface, where the design process was still slowly converging to the targets. The slight roughness in the design pressures just ahead of the trailing edge on each surface is attributable to the flow solver rather than to the design process. The resulting lift and pitching-moment coefficients of 0.602 and -0.148, respectively, meet the specified flow constraints. Although a weak shock is evident in the pressure distribution, it generates less than half a count (0.00005) of wave drag, thus satisfying the wave-drag constraint. The final airfoil geometry is plotted in figure 7(b). The maximum thickness-chord ratio of 0.118 is very close to the desired value of 0.120, whereas the leading-edge-radius value of 0.013 is about 20 percent below the target of 0.016. The airfoil resembles current supercritical airfoils with mild aft camber.

Since the method for automatically generating target pressures was developed primarily for airfoils at transonic speeds, this good agreement is not surprising. For more conventional airfoils or for lower speeds, the initial targets developed may not yield as close a match to the geometric constraints. This possibility emphasizes the need for a method to automatically modify the target pressures during a design run, and this is discussed in a subsequent section of this paper.

Control Point Fitting Approach

The control point fitting approach is especially useful when the design problem involves the modification of an initial configuration to satisfy a set of constraint values. This approach differs from the empirical estimation approach in that the initial levels and, in general, the positions for the control points are based on the pressure distribution for the original airfoil at the design conditions rather than on empirical relationships for a class of airfoils. The criteria for determining the locations of the control points are described below.

Determination of control point locations and levels. Control point 1 corresponds to the leading edge of the airfoil, or to the stagnation point if it does not occur at the leading edge. Its location is determined by finding the beginning of the first favorable pressure gradient on each surface. The location of point 2 corresponds to the end of this initial rapid acceleration region (defined as the first

point where $dC_p/dx \geq -10$) or where $x \geq 0.1$, whichever occurs first. Control points 3 and 4 are arbitrarily located at $x = 0.3$ unless a shock is detected. A shock is defined to be present when $dC_p/dx \geq 5$ in a region of supersonic flow over the airfoil. In this case, control point 3 is moved to the location at the beginning of this adverse pressure gradient, representing the head of the shock. Point 4 is then placed at the foot of the shock, which for the DGAUSS shock-fitting code is always the next grid point. For shock-capturing codes, which have a tendency to smear shocks, an alternate criterion could be used such as the next point with a subsonic local Mach number. Control point 5 is located at $x = 0.4$ or at the next analysis point past point 4, whichever is farther aft. Control point 6 corresponds approximately to the beginning of the final pressure-recovery region. Since there can be a wide variety of pressure gradients in this region, including a favorable gradient on the lower surface for a supercritical airfoil, no attempt was made to define a flow criterion for locating this point; instead, control point 6 was placed at $x = 0.85$ based on the observed characteristics of supercritical airfoils. The final control point on each surface is always located at the trailing edge.

Although the method described above generally gives satisfactory results, certain pressure distributions may require manual adjustments to some of the control point locations to provide a better match with the initial pressure distribution. An example of this would be shifting control point 6 on the lower surface to coincide with the maximum cove pressure on a supercritical airfoil. Also, the pressure distribution from the initial analysis may be altered before the fitting procedure is applied in order to obtain characteristics such as an alternate shock location.

The pressure levels at these control points are initially set to the values of the corresponding points on the analysis pressure distribution for the original airfoil. Since this pressure distribution was obtained for an airfoil with a known maximum thickness, the coefficient A in equation (8) can be recalibrated by using the average pressure level at point 5 for the current case. Designing for a desired airfoil thickness then involves only a small perturbation from a known value rather than an estimate based on general airfoil characteristics, as in the empirical estimation approach.

The detailed target values between the control points can be specified either by using analytic functions as in the empirical estimation approach or by simply retaining the values of the analysis pressures. The latter method tends to preserve the characteristics of the original airfoil, and for small changes it is the preferred approach. To satisfy the flow constraints, the pressure levels at selected control points are automatically adjusted as in the empirical estimation approach. The detailed target values between control points are then recomputed if analytic functions are used, or they are simply adjusted using linear shearing if the original pressures were retained in the initial target distribution.

Example using target-fitting approach. To illustrate the target-fitting approach, an airfoil was designed to the same lift, wave-drag, and pitching-moment constraints used in the empirical estimation method, but with the free-stream Mach number increased to 0.77 and the thickness-chord ratio reduced to 0.10. A Reynolds number of 10×10^6 was used for the boundary-layer computation. The final airfoil from the empirical estimation case is used to initiate the target-fitting approach and subsequent design process. Figure 8 shows the pressure distribution resulting from an analysis of this airfoil at the new design Mach number of 0.77 and lift coefficient of 0.6. Note that the shock has moved aft and is stronger than the final design pressure distribution at $M = 0.75$ (fig. 7(a)). This results in a wave-drag coefficient of 0.0024 and a pitching-moment coefficient of -0.164, both of which violate the constraint values of 0.0005 and -0.150.

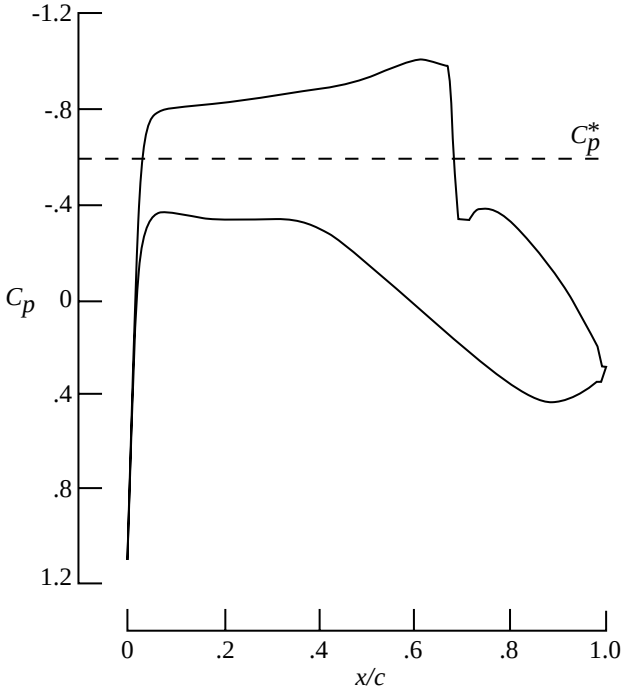

Figure 8. Pressure distribution from analysis for $M_\infty = 0.77$ and $c_l = 0.6$ of airfoil designed for $M_\infty = 0.75$ and $c_l = 0.6$.

The target-fitting approach described above was applied to these pressures, with the segments between control points defined using the original pressures instead of analytic functions. These control points were adjusted to meet the constraints, and the resulting detailed target distribution as well as control point values are shown in figure 9. The DGAUSS code was then used in the basic DISC mode to modify the initial airfoil to match this new detailed target distribution. As can be seen in figure 10(a), the final design pressures accurately match the target distribution. The resulting lift, wave-drag, and pitching-moment coefficients of 0.600, 0.0005, and −0.151, respectively, are satisfactory. The final airfoil is compared with the initial shape in figure 10(b). The maximum thickness-chord ratio was reduced from 0.118 to 0.103, or slightly thicker than the target value of 0.100. Although no constraint on leading-edge radius was included in this design, the radius was found to decrease from the initial airfoil in a proportion that was consistent with the thickness reduction.

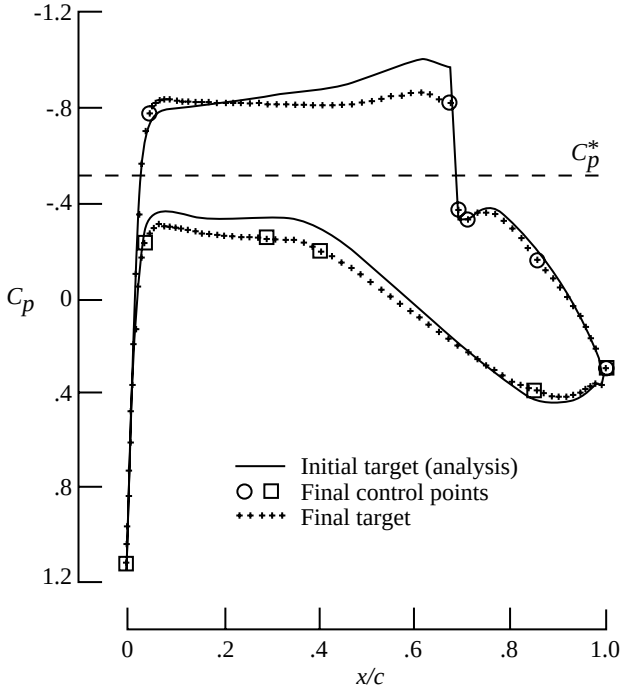

Figure 9. Target pressures from control point fitting approach for $M_\infty = 0.77$ and $c_l = 0.6$.

CDISC Automated Method for Modifying Target Pressure

The above examples demonstrate that the automated methods can generate target pressures that will meet the flow constraints and produce airfoils having geometric characteristics close to the desired values. In order to match the geometric constraints more closely, however, especially for thin or very thick airfoils, the following method was implemented for automatically modifying the target pressures during the design process.

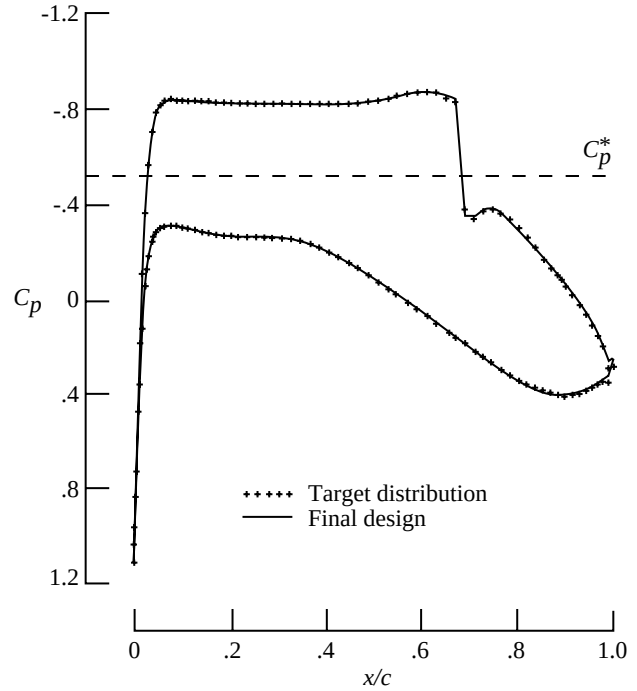

(a) Pressure distribution.

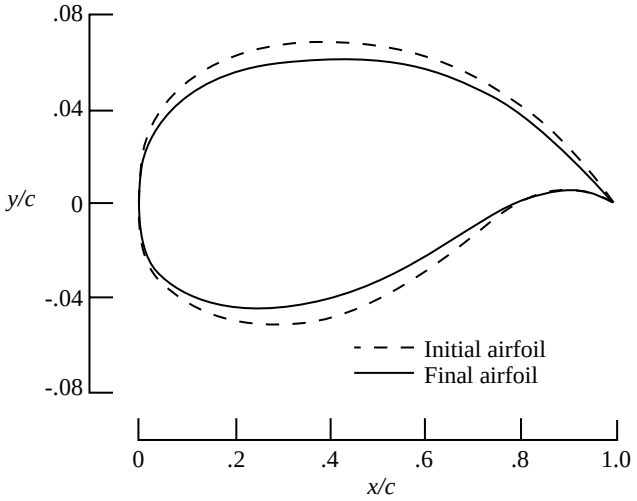

(b) Airfoil.

Figure 10. Basic DISC design results from control point fitting approach for $M_\infty = 0.77$ and $c_l = 0.6$.

Modification of Control Point Locations and Levels

The constrained DISC (CDISC) method has been developed to automatically modify the initial target pressures during a design run in order to meet both flow and geometric constraints. This method

for target pressure modification is similar to the empirical estimation approach for target generation in that it utilizes specified pressure-geometry relationships. The main difference is that when modifying the target pressures, perturbation forms of the equations are used instead of the absolute relationships developed for target generation since the geometric parameters corresponding to the current target pressures are known. For example, the relationship between maximum airfoil thickness and the average pressure level at control point 5 given in equation (8) becomes

$$\Delta C_p = \frac{A(\Delta t/c)}{\sqrt{1 - M_\infty^2}} \tag{16}$$

where $\Delta t/c$ is the difference between the desired and current airfoil maximum thickness-chord ratios and ΔC_p is the required change to the pressure coefficient of control point 5 on each surface. Although a direct differentiation of equation (8) yields $A = -3.3$, a value of -6.0 has been found to result in faster convergence. Equation (16) is generally valid except in the immediate vicinity of the leading and trailing edges. In addition to controlling the global parameter of maximum thickness, equation (16) is used to enforce a minimum local thickness constraint at the average chord location for control point 6.

The leading-edge radius of the airfoil is altered by changing the chordwise locations rather than the pressure levels of control point 2. A forward shift of the points will result in a blunter airfoil, whereas a location farther aft will reduce the nose radius. The required movement for the points is estimated from the equation

$$\Delta x = 0.0002\ \Delta C_{le} \tag{17}$$

where C_{le} is the magnitude of the leading-edge curvature (the reciprocal of the radius) and ΔC_{le} is the difference between the desired and current values.

After the new control point locations for meeting the thickness and radius constraints have been determined, the detailed target distributions must be adjusted accordingly. If the pressures between control points have been defined using analytic functions, the new levels are simply recomputed by using the new end points for the same functions. If the target-fitting approach is used, the new levels associated with the thickness changes are obtained by using a linear shearing as in the target generation. For the leading-edge-radius adjustment, the detailed pressures are modified in a two-step process. First, the x's for the points between control points 1 and 3 are linearly incremented, based on the change at control point 2, while the pressure level associated with each point is held constant. Since the current implementation of the DISC design method expects the target pressures to be specified at the grid point locations, a second step is required in which the pressure coefficients at the original streamwise locations are interpolated from the new distribution. After all these geometry-related modifications have been made, the pressure levels at control points 2, 3, 4, and 6 are adjusted to satisfy the flow constraints.

Figure 11 illustrates how the CDISC method for modifying the target pressures has been incorporated into the basic DISC design method. After every third call to the DISC design module, the geometric parameters for the current airfoil are determined and passed to the target modification module where the appropriate adjustments are made to the control points and detailed target pressures. The new detailed target is then passed back to the design module for use in the next design update. This approach allows the flow solution, airfoil design, and target specification to converge in parallel, thus reducing the computer resources required.

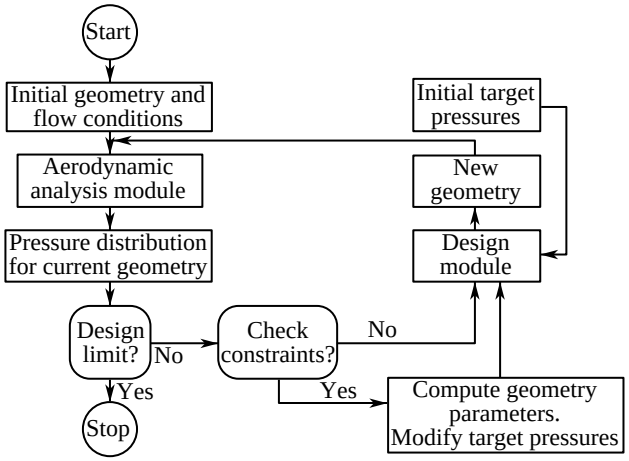

Figure 11. Flowchart of CDISC design method.

Example Using CDISC Target Modification Approach

As an illustration of this approach, the CDISC method was applied to the target from the target-fitting design example (see fig. 10) in an effort to match the geometric constraints more closely. As the design proceeds, this distribution is adjusted based on the current geometric parameters, and it eventually arrives at the final target shown in figure 12. The final design pressures match this target very well (fig. 13(a)) and all the flow constraints are met. The initial and final airfoils from the design are compared in figure 13(b). The maximum airfoil thickness-chord ratio was reduced from 0.103 to the desired value

of 0.100, and the leading-edge radius was increased from 0.0073 to 0.0107, close to the constraint value of 0.0110. A third geometric constraint was imposed to maintain the thickness of the initial airfoil at the location of control point 6, that is, $x = 0.85$. The final thickness at this location was within $\pm 0.0004c$ of the specified value. Since relatively minor changes to the initial target distribution were required, the CDISC design process required the same amount of computer time as the basic DISC design in the target-fitting example (approximately 143 cpu seconds on a Cray Y-MP computer).

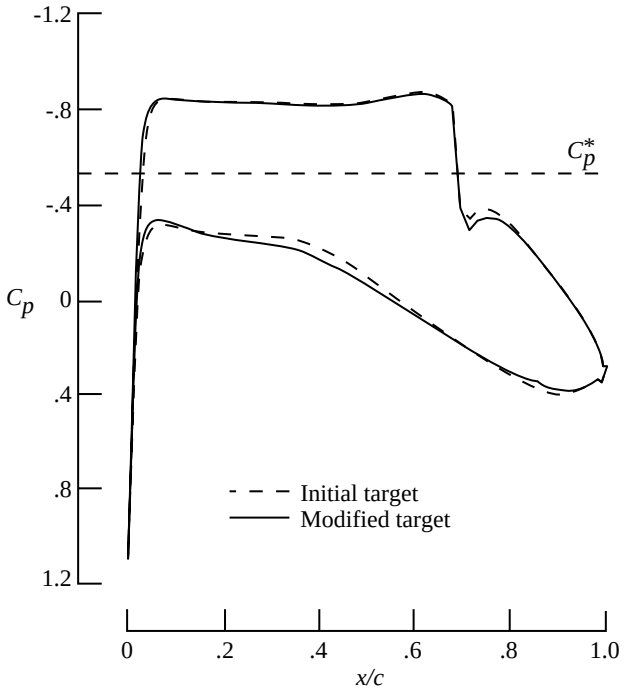

Figure 12. Target pressures from CDISC design case for $M_\infty = 0.77$ and $c_l = 0.6$.

Glove Constraint Option and Example

An additional geometric constraint implemented in the CDISC approach is the "glove" option. In this option, the design surface geometry is required to remain between inner and outer bounding surfaces over a specified chordwise region. This capability would be used, for example, in the design of a wing glove for flight research where the new geometry must lie outside the existing wing shape or spar box, or for developing an efficient external shape that encloses an internal aircraft component such as an antenna. Although this set of constraints could be addressed directly by restricting the aerodynamic surface coordinates from penetrating the bounding surfaces, this approach would allow little, if any, control over the resulting flow characteristics. Therefore, an indirect approach involving target pressure alteration was developed.

The detailed target pressures are modified using a pressure-geometry relationship similar to that of equation (16), except that a desired change in surface ordinate is used instead of a change in thickness, and the coefficient A changes sign for the lower surface of an airfoil. Although strictly valid only for subsonic flow, this relationship has also been used successfully in mildly supercritical flow.

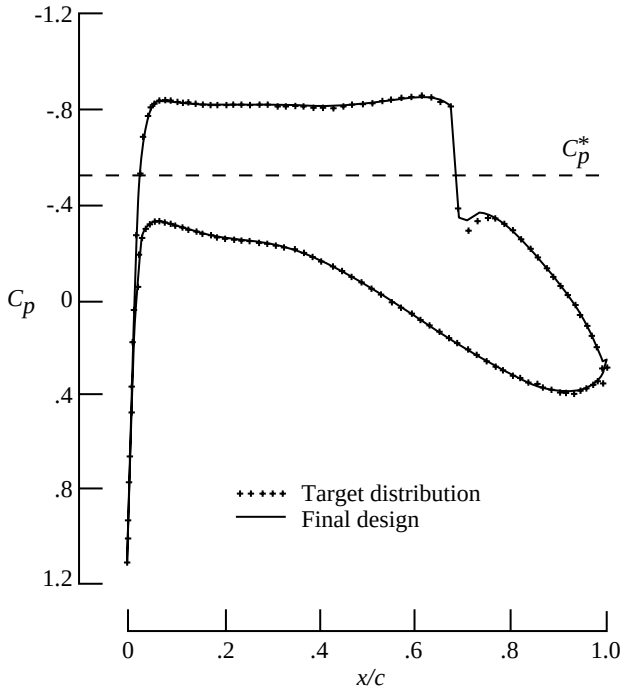

(a) Pressure distribution.

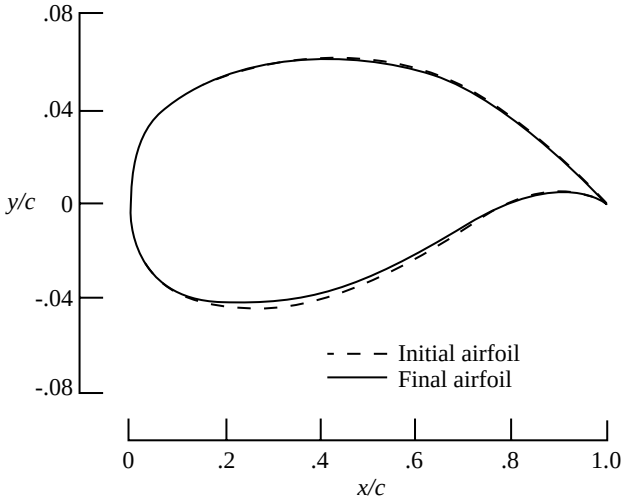

(b) Airfoil.

Figure 13. CDISC design results for $M_\infty = 0.77$ and $c_l = 0.6$.

Three approaches for altering the detailed target pressure distribution are investigated. The first approach simply checks for penetration of the bounding surface at each point in the constraint region and adjusts the pressure coefficient locally based on the magnitude of the penetration. An alternative approach is to determine the maximum penetration distance and adjust all the target pressures over the constraint region by a constant increment based on that distance. This approach is useful for cases where maintaining a specified gradient in the target pressures is desirable, as in laminar flow designs. The third approach is a modification of the constant increment procedure that uses a linearly varying increment. With this approach, one end of the segment of the pressure distribution over the constraint region is fixed and the rest of the segment is linearly sheared to meet the no-penetration criteria. This approach can yield the maximum favorable gradient that satisfies both the geometric constraint and a wave-drag constraint.

To illustrate these approaches, a natural laminar flow (NLF) glove was designed for an airfoil. This case represents an automated approach to the Variable Sweep Transition Flight Experiment (VSTFE) design exercise using an F-14 reported by Waggoner, Campbell, and Phillips (1985), which required numerous manual modifications to the target pressures as well as airfoil geometries to develop glove shapes that met both the flow and geometric constraints. At the wing station selected for this case, the glove began $0.02c$ ahead of the leading edge of the baseline airfoil and extended to $x/c = 0.58$ on the upper surface and to $x/c = 0.30$ on the lower surface. Since the actual glove on the upper surface terminated in an aft-facing step, a computational fairing was included by extending the upper surface design region to $x/c = 0.70$.

In addition to the chordwise extent of the design region, geometric constraints were imposed by the existing airfoil shape and allowable glove thicknesses. These constraints were used to develop inner and outer bounding surfaces for constrained design. The baseline airfoil coordinates comprised the inner bounding surface except on the upper surface ahead of $x/c = 0.50$ where $0.0065c$ was added to the ordinates to allow for installation of pressure measurement tubes. The original design constraints required that the glove thickness at $x/c = 0.58$ on the upper surface be no more than $0.01c$ to reduce any adverse effects caused by the aft-facing step. A more conservative maximum glove thickness of $0.005c$ was used from $x/c = 0.58$ to 0.70 in order to demonstrate the outer bounding surface capability.

The main flow constraint for this case was to avoid an adverse pressure gradient over the front half of the upper surface so that natural laminar flow could be maintained in this region. This constraint was to be met at the design lift coefficient with no shock development. A target pressure distribution was generated by first analyzing the initial airfoil at the two-dimensional design conditions of $M_\infty = 0.65$ and $c_l = 0.6$. This distribution was then modified on the upper surface by specifying a quartic distribution of pressure coefficients between the leading edge and $x/c = 0.01$, followed by a pressure coefficient gradient of -0.05 aft to $x/c = 0.50$. (See fig. 14.) This favorable gradient was deliberately chosen to represent a design case that was more difficult than the neutral gradient cases reported by Waggoner, Campbell, and Phillips (1985). The initial pressure levels in this region were adjusted to match the original lift coefficient of 0.6.

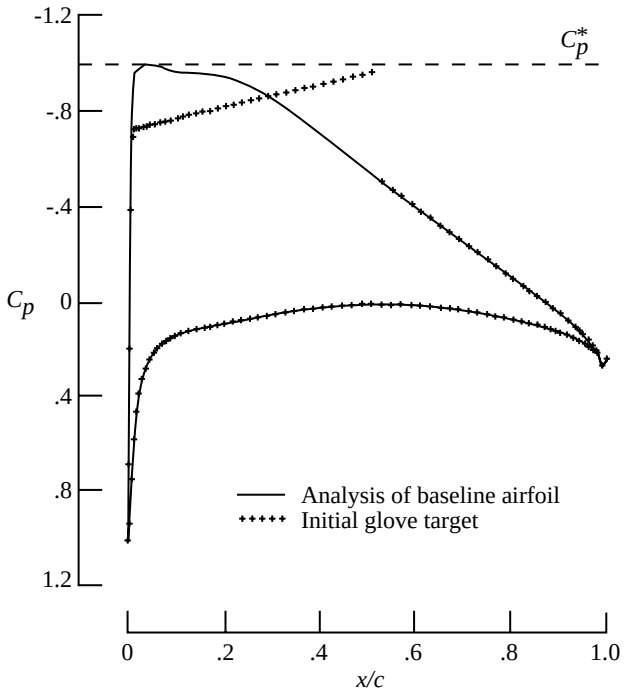

Figure 14. Pressure distribution of initial glove target for $M_\infty = 0.65$.

The initial airfoil for the design was developed by linearly shearing the coordinates of the baseline airfoil in the design region on each surface to extend forward to the leading edge of the glove. This airfoil was then translated and nondimensionalized so that the leading and trailing edges were again at $x/c = 0$ and 1.0, respectively. Finally, these coordinates were smoothed to blend the stretched regions into the original airfoil.

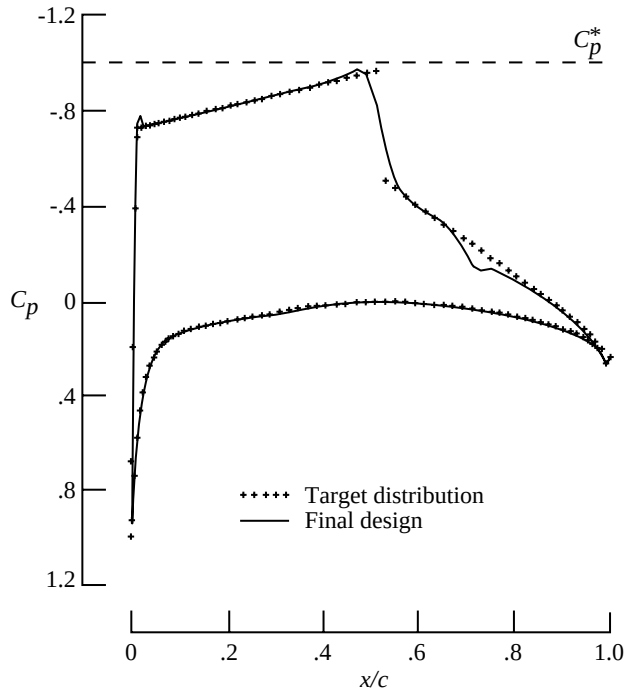

(a) Pressure distribution.

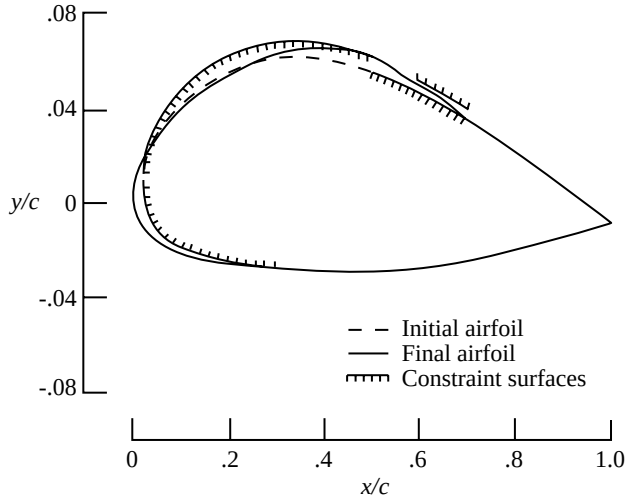

(b) Airfoil.

Figure 15. Results of basic (unconstrained) DISC design for initial glove target for $M_\infty = 0.65$.

The code was first run in the basic DISC design mode to match the initial target pressure distribution. As shown in figure 15(a), the final pressures match the target values fairly well on the lower surface and over the constant gradient portion of the upper surface. On the upper surface, slight overshoots of the targets occur at the beginning and end of the constant gradient region. The steep recovery gradient near midchord has been reduced as a result of the airfoil smoothing done during the design. A mismatch between target and design pressures also occurs at the end of the design region ($x/c = 0.70$), thus indicating a discontinuity in curvature at this point. Again, since the actual flight glove would end at $x/c = 0.58$, this discrepancy is not significant. A comparison of the resulting design geometry with the bounding surfaces (fig. 15(b)) shows that the inner surface constraint is violated on the upper surface over most of the front half of the chord.

The design was therefore repeated by using the glove constraint option. All three pressure modification approaches were used in this example. On the upper surface, the constant gradient method was used ahead of $x/c = 0.50$, with smoothing used to blend the steep leading-edge acceleration into the mild favorable gradient as the level was adjusted. Between $x/c = 0.50$ and 0.70, the linearly varying increment approach (with the aft end of the target segment fixed) was used to ensure that the pressures matched those for the initial target at the end of the design region. On the lower surface, the individual point adjustment technique was used, again with smoothing employed to fair into the fixed portion of the target distribution.

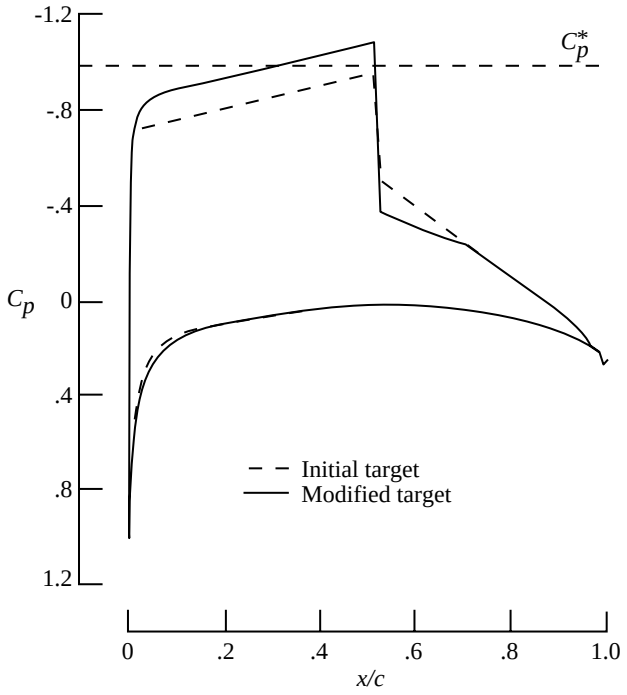

Figure 16. Target pressures from CDISC glove design for $M_\infty = 0.65$.

The modifications made by the design code to the initial target pressures are shown in figure 16. The inner surface constraint drove the level of the constant gradient section on the upper surface toward more

negative pressure coefficients, whereas the outer surface constraint caused a reduction in the adverse gradient aft of midchord. These modifications resulted in a net increase in lift for the airfoil section. If a constant lift coefficient requirement is imposed, one or more of the other flow constraints (such as the chordwise extent of the constant favorable gradient region) must be compromised. Figure 17(a) indicates that the agreement between the final design and target pressures is similar in character to that seen in figure 15(a) for the basic DISC design, with the exception that the overshoot at the beginning of the constant gradient region has been eliminated. Moreover, examination of the final airfoil geometry in figure 17(b) reveals that it satisfies both the inner and outer bounding surface constraints.

SCR Minimization Approach and Example

As mentioned in the section on the generation of target pressures, the requested values of the global design variables, along with the limitations imposed to ensure a reasonable pressure distribution, may overconstrain the process of developing the targets. In such cases, a strategy must be defined for relaxing the constraints in a manner that has a minimum adverse effect on the design. One such approach is the successive constraint release (SCR) method, in which a one-sided constraint is incrementally released until the minimum value is found that will allow the other constraints to be met. For example, a lift constraint violation can be relieved either by increasing the wave-drag limit so that more lift can be carried over the forward portion of the airfoil or by relaxing the pitching-moment constraint and thus increasing the aft loading. This method becomes a constrained minimization technique when a variable is set to the minimum possible value (i.e., $c_{d,w} = 0$) and is then released until the other constraints (lift and pitching moment) are satisfied. The design variable that is released would thus correspond to the objective function in numerical optimization.

The SCR approach has been incorporated into the empirical estimation method for generating target pressures. Three objective functions to be minimized are available: $|c_m|, c_{d,w}$, and $\tilde{c}_d$. The third function ($\tilde{c}_d$) is a composite drag variable that includes an estimate of the trim drag based on the value of the pitching-moment coefficient. The equation for this function is

$$\tilde{c}_d = c_{d,w} + c_1 \, |c_m| \qquad (18)$$

where the constant c_1 depends on the longitudinal stability characteristics of the aircraft, with a typical value being on the order of 0.01.

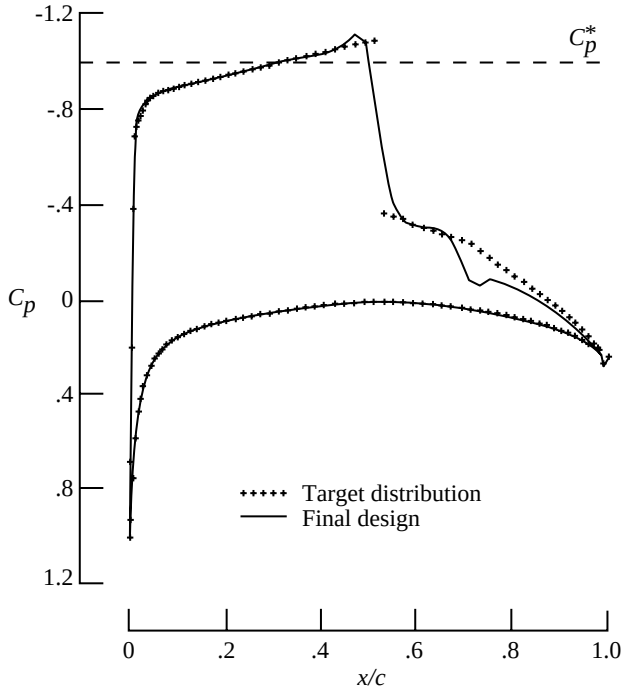

(a) Pressure distribution.

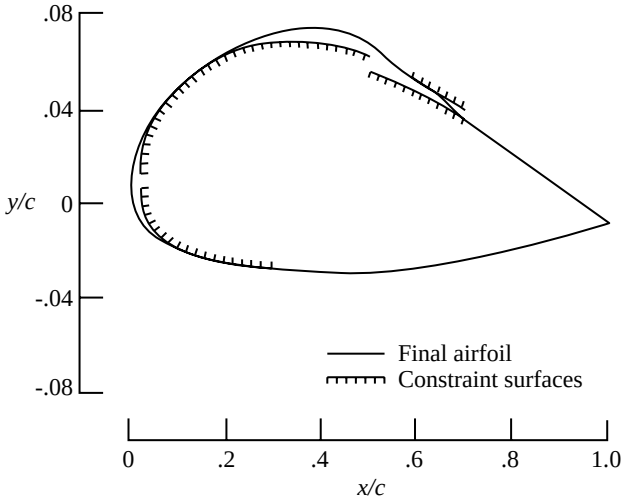

(b) Airfoil.

Figure 17. Results from CDISC glove design for $M_\infty = 0.65$.

Minimizing the magnitude of the pitching-moment coefficient is simply a matter of releasing that constraint while holding the lift and wave-drag constraints fixed. In minimizing the wave-drag coefficient, however, releasing only the value of $c_{d,w}$ will not always allow the pitching-moment constraint to be met. This situation occurs when

the shock location (control point 3) is at or aft of $x = 0.5 - (x_2)_{\text{upper}}$. For this shock location, the increase in lift between points 2 and 3 on the upper surface due to releasing the wave-drag constraint is balanced about the moment reference center ($x = 0.25$), with the result that no change in pitching moment occurs. For these cases, the pitching-moment constraint must also be relaxed. In minimizing the third objective function ($\tilde{c}_d$), the wave drag and pitching moment are initially set to 0, and then the pitching-moment coefficient is released until the remaining constraints are satisfied. The wave-drag coefficient is then incremented and the pitching moment is again minimized. This process continues as long as the resulting values of $\tilde{c}_d$ are decreasing. This termination criterion assumes that the first minimum encountered is an absolute minimum. This criterion has also been altered to explore a broader matrix of wave drag and pitching moment to ensure that the true minimum is found, but experience thus far has indicated that the original assumption is valid.

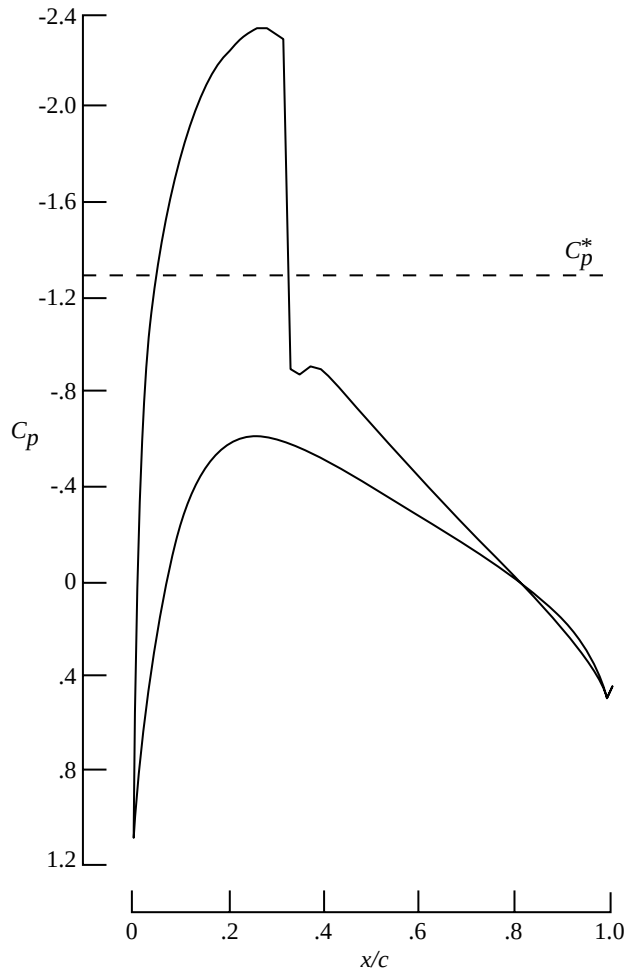

Figure 18. Analysis of NACA 0025 airfoil at $M_\infty = 0.6$ and $c_l = 0.6$.

The procedures described above minimize the objective functions for a given shock location. In order to provide a more general minimization capability, an option has been included for automatically determining the minimum value of the functions over a range of shock locations. A default range is defined as $0.1c$ forward and aft of the estimated shock location given by equation (10).

To illustrate the constrained minimization capability, a 25-percent-thick airfoil was designed at $M_\infty = 0.6$ and $c_l = 0.6$ with the objective of minimizing $\tilde{c}_d$. (For this case, c_1 was arbitrarily set to 0.01.) The airfoil thickness was selected as being representative of an advanced-technology, high-altitude, long-endurance aircraft (Hall 1990), and therefore it should provide a good indication of the generality of the empirical relationships used to generate the initial target pressures. Although wave drag would not ordinarily be a concern at this design Mach number, the large thickness-chord ratio and moderate lift coefficient could easily result in transonic flow. For example, analysis of an NACA 0025 airfoil at the design Mach number and lift coefficient shows that a strong shock is present near $x/c = 0.3$ (fig. 18), thus resulting in a wave-drag coefficient of 0.0057.

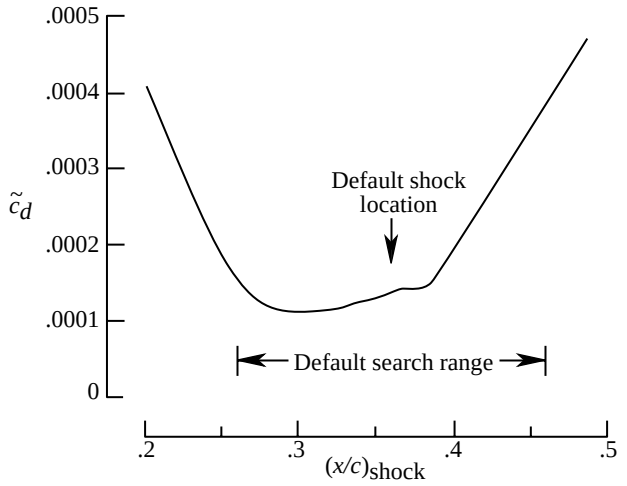

Figure 19. Minimum values of composite drag function for various shock locations for a 25-percent-thick airfoil at $M_\infty = 0.6$ and $c_l = 0.6$.

The SCR method was used to generate the initial target pressures for this case. Figure 19 shows the values of $\tilde{c}_d$ obtained by this minimization process for shock locations ranging from $x/c = 0.2$ to 0.5. The minimum value for $\tilde{c}_d$ of about 0.0001 was found to occur near $x/c = 0.3$. The curve has a very shallow character, however, so that the shock can be placed anywhere between $x/c = 0.25$ and 0.40 and still be within ± 0.0001 of the minimum. Note that

the default shock location of $x/c = 0.36$ determined from equation (10) is within this region, and that this region would be included in the default shock-search range of $x/c = 0.26$ to 0.46.

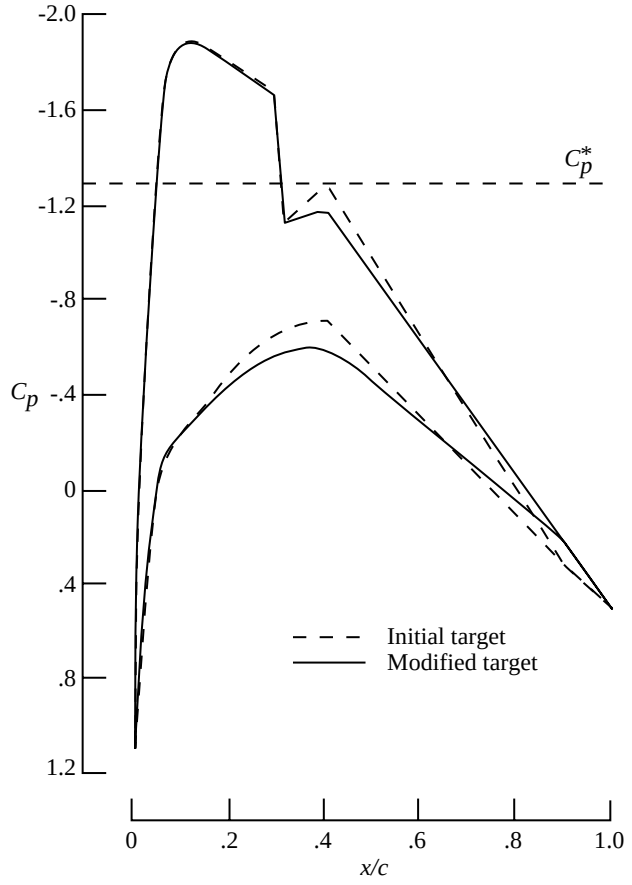

Figure 20. Target modifications for constrained minimization case at $M_\infty = 0.6$ and $c_l = 0.6$.

The control point values corresponding to the minimum $\tilde{c}_d$ shock location ($x/c = 0.31$) were used to initiate the constrained design process. The wave-drag and pitching-moment constraint values computed by the minimization process for this condition were 0.00003 and -0.010, respectively. The fifth decimal place in the drag coefficient was not significant from an accuracy standpoint but was included to indicate that a weak shock was allowed. Additional geometry constraints were enforced to maintain the leading-edge radius and the thickness at $x/c = 0.9$ of the initial airfoil.

In principle, the entire minimization procedure should have been repeated during the design process when the target distribution was modified to reflect the actual values of the geometric design variables. This capability has not been incorporated into the DGAUSS code yet; however, since the "optimum" curve for this case was fairly shallow, holding the shock location fixed probably did not adversely affect the design results. If constraint violations had occurred during the design, the pitching-moment limit could have been relaxed to allow the other constraints to be met.

The CDISC design process was initiated by using an NACA 0025 airfoil. The initial and final targets from the design are shown in figure 20. The changes in the midchord region indicate that the initial levels for the maximum-thickness control points were too negative and thus produced an airfoil that was too thick. Furthermore, the initial targets caused the airfoil to be too thin at $x/c = 0.9$ during the early stages of the design, with the result that the average pressure coefficient at that location had to be decreased. Even with these adjustments, the other constraints could be met without requiring the pitching-moment limit to be released.

The pressures from the final design cycle are compared with final target distribution in figure 21(a). The agreement in general is excellent, with the only significant discrepancy occurring close to the shock where the actual shock is slightly weaker than the target value. The computed lift and pitching-moment coefficients match their respective target values of 0.600 and -0.010 within ± 0.001. Essentially no wave drag was produced by the weak shock, and thus the resulting value of $\tilde{c}_d$ matched the specified level of 0.0001.

The final airfoil geometry is compared with the initial NACA 0025 shape in figure 21(b). The new design matches the desired maximum thickness-chord ratio of 0.250 and maintains the thickness of the original airfoil at $x/c = 0.9$. The leading-edge shape appears to be very similar to the initial geometry, but it is about 10 percent less blunt with a radius of $0.063c$. From an aerodynamic standpoint, the smaller radius is not a problem and would probably improve the overall performance of the airfoil.

Finally, it should be noted that although an interacted boundary-layer computation for a chord Reynolds number of 10×10^6 is included in this design, the accuracy of the viscous effects is questionable. The boundary-layer computation predicts that flow separation occurs at about $x/c = 0.82$ on the upper surface. Although the simple boundary-layer method used in this case continued to calculate a displacement thickness beyond this point, the results are dubious since no separated-flow model is included. Obviously, viscous criteria would have to be included in the actual design of such an airfoil. Within this limitation, however, the SCR-

constrained minimization approach did succeed in producing a very reasonable airfoil geometry that, in general, met the constraints and objectives and required only global design parameters as input.

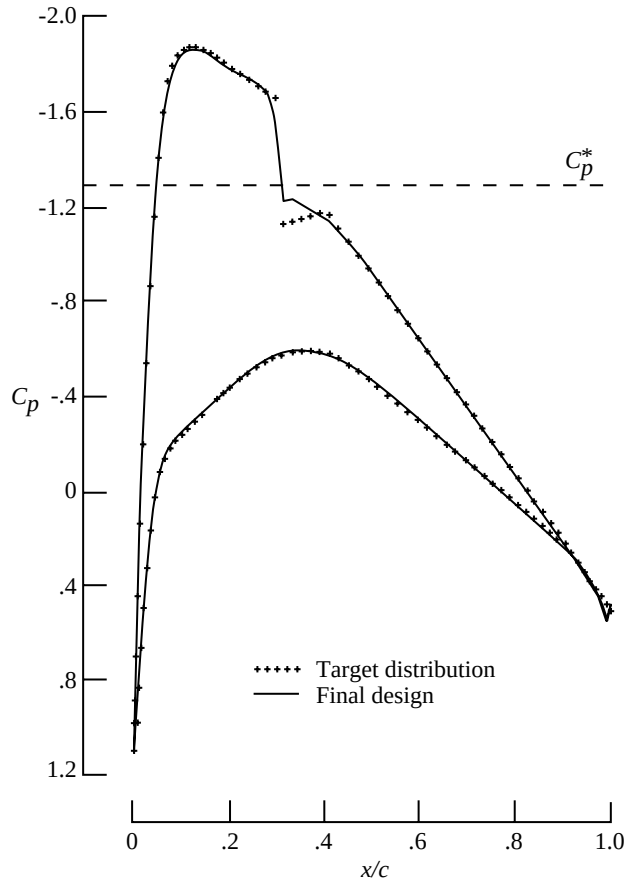

(a) Pressure distribution.

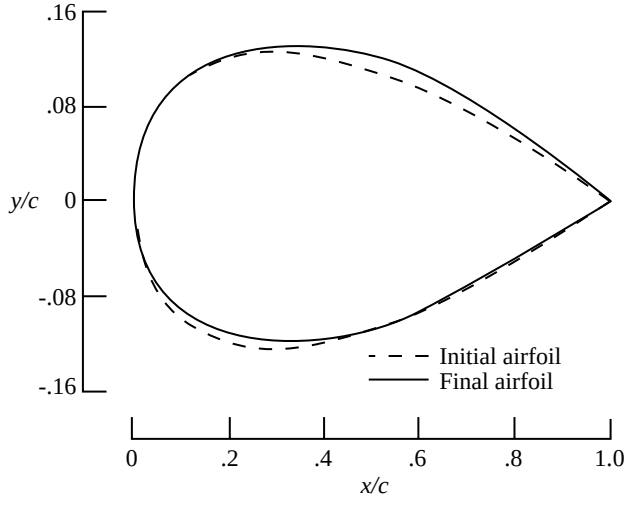

(b) Airfoil.

Figure 21. CDISC design results for constrained minimization case at $M_\infty = 0.6$ and $c_l = 0.6$.

Concluding Remarks

An approach has been developed for incorporating flow and geometric constraints into the basic Direct Iterative Surface Curvature (DISC) design method. In this approach, an initial target pressure distribution was developed using a set of control points. The chordwise locations and pressure levels of these points were initially estimated either from empirical relationships and observed characteristics of pressure distributions for a given class of airfoils or by fitting the points to an existing pressure distribution. These values were then automatically adjusted during the design process to satisfy the flow and geometric constraints. The constraint options currently available include flow parameters such as lift, wave drag, and pitching moment, and also geometric parameters such as maximum thickness, local thickness, and leading-edge radius. This approach has also been extended to include the successive constraint release (SCR) approach to constrained minimization.

Test cases were included to illustrate both the empirical estimation and the control point fitting approaches to target pressure generation. Basic DISC design results for each approach indicated that the flow parameters for the final design met the requirements and that the geometric parameters were fairly close to the desired values. Thus, either method could be used to generate a good initial target distribution.

The constrained DISC (CDISC) method which adjusts the target pressures during the design process was then applied to the control point fitting approach listed above. In this example, the constrained design procedure produced an airfoil that accurately matched the desired geometric values while maintaining good agreement with the flow constraints. Since relatively minor changes to the initial target distribution were required and a simultaneous flow, design, and target convergence approach was used, the CDISC design process required about the same amount of computer time as the basic DISC design.

An example of a second constrained design was given to illustrate a "glove" constraint capability. The results showed that the specified favorable pressure gradient over the front half of the upper surface of the airfoil was maintained and that the inner and outer bounding surface constraints were not violated.

The final example of a constrained design demonstrated the SCR minimization approach applied to the design of a thick airfoil. The SCR approach was used in conjunction with the empirical estimation approach to define an initial target distribution with a shock location, wave drag, and pitching moment

that yielded the minimum value of a composite drag objective function. The constrained design process did not make large changes to the target pressures, thus indicating that the empirical relationships used to generate the initial target may be used for a wide range of airfoil thicknesses. The final design met all the constraints.

The CDISC design method in combination with the SCR minimization approach thus offers an efficient and accurate approach to aerodynamic design. Since the target pressure generation and modification are automated and require only global parameters as input, the amount of manual intervention needed is greatly reduced. Also, the simultaneous convergence of the flow field, design geometry, and target pressures allows the constrained designs to be obtained very efficiently. This efficiency, along with the use of global design variables, makes the CDISC approach an attractive alternative to numerical optimization. Finally, although this report demonstrates only the capabilities for airfoil design, the concepts are amenable to three-dimensional design problems.

NASA Langley Research Center
Hampton, VA 23681-0001
September 30, 1992

References

Anon. 1990a: *Computational Methods for Aerodynamic Design (Inverse) and Optimization.* AGARD-CP-463.

Anon. 1990b: *Special Course on Inverse Methods for Airfoil Design for Aeronautical and Turbomachinery Applications.* AGARD-R-780.

Bell, R. A.; and Cedar, R. D. 1991: An Inverse Method for the Aerodynamic Design of Three-Dimensional Aircraft Engine Nacelles. *Proceedings—Third International Conference on Inverse Design Concepts and Optimization in Engineering Sciences—ICIDES-III* George S. Dulikravich, ed., Pennsylvania State Univ., pp. 405–417.

Campbell, Richard L.; and Smith, Leigh A. 1987a: *Design of Transonic Airfoils and Wings Using a Hybrid Design Algorithm.* SAE Tech. Paper Ser. 871756.

Campbell, Richard L.; and Smith, Leigh A. 1987b: A Hybrid Algorithm for Transonic Airfoil and Wing Design. *A Collection of Technical Papers—AIAA 5th Applied Aerodynamics Conference,* American Inst. of Aeronautics and Astronautics, pp. 527–538. (Available as AIAA-87-2552.)

Dulikravich, George S. 1990: Aerodynamic Shape Design. *Special Course on Inverse Methods for Airfoil Design for Aeronautical and Turbomachinery Applications,* AGARD-R-780, pp. 1-1–1-10.

Giles, Michael; and Drela, Mark 1986: A Two-Dimensional Transonic Aerodynamic Design Method. *A Collection of Technical Papers, AIAA 4th Applied Aerodynamics Conference,* American Inst. of Aeronautics and Astronautics, pp. 197–204. (Available as AIAA-86-1793.)

Hall, Douglas R. 1990: Thick Airfoil Designs for a Hale Vehicle. *A Collection of Technical Papers, Part 1—AIAA 8th Applied Aerodynamics Conference,* pp. 323–331. (Available as AIAA-90-3036-CP.)

Hartwich, Peter-M. 1990: Fresh Look at Floating Shock Fitting. AIAA-90-0108.

Hicks, Raymond M.; Murman, Earll M.; and Vanderplaats, Garret N. 1974: *An Assessment of Airfoil Design by Numerical Optimization.* NASA TM X-3092.

Lin, W. F.; Chen, A. W.; and Tinoco, E. N. 1990: 3D Transonic Nacelle and Winglet Design. *A Collection of Technical Papers, Part 2—AIAA 8th Applied Aerodynamics Conference,* pp. 582–591. (Available as AIAA-90-3064.)

Lock, R. C. 1985: Prediction of the Drag of Wings at Subsonic Speeds by Viscous/Inviscid Interaction Techniques. *Aircraft Drag Prediction and Reduction,* AGARD-R-723, pp. 10-1–10-71.

Malone, J. B.; Narramore, J. C.; and Sankar, L. N. 1990: An Efficient Airfoil Design Method Using the Navier-Stokes Equations. *Computational Methods for Aerodynamic Design (Inverse) and Optimization,* AGARD-CP-463, pp. 5-1–5-18.

Nash, J. F.; and Macdonald, A. G. J. 1967: *The Calculation of Momentum Thickness in a Turbulent Boundary Layer at Mach Numbers up to Unity.* C.P. No. 963, British Aeronautical Research Council.

Oswatitsch, Klaus (English version by Gustav Kuerti) 1956: *Gas Dynamics.* Volume I of *Applied Mathematics and Mechanics,* Academic Press, Inc., pp. 447–497.

Smith, Leigh Ann; and Campbell, Richard L. 1991: *A Method for the Design of Transonic Flexible Wings.* NASA TP-3045.

Sobieczky, H.; Yu, N. J.; Fung, K.-Y.; and Seebass, A. R. 1979: New Method for Designing Shock-Free Transonic Configurations. *AIAA J.,* vol. 17, no. 7, pp. 722–729.

Squire, H. B.; and Young, A. D. 1938: *The Calculation of the Profile Drag of Aerofoils.* R. & M. No. 1838, British Aeronautical Research Council.

Stratford, B. S.; and Beavers, G. S. 1961: *The Calculation of the Compressible Turbulent Boundary Layer in an Arbitrary Pressure Gradient—A Correlation of Certain Previous Methods.* R. & M. No. 3207, British Aeronautical Research Council.

Van den Dam, R. F.; Van Egmond, J. A.; and Slooff, J. W. 1990: Optimization of Target Pressure Distributions. *Special Course on Inverse Methods for Airfoil Design for Aeronautical and Turbomachinery Applications,* AGARD-R-780, pp. 3-1–3-13.

Van Egmond, J. A. 1990: Numerical Optimization of Target Pressure Distributions for Subsonic and Transonic Airfoil Design. *Computational Methods for Aerodynamic Design (Inverse) and Optimization,* AGARD-CP-463, pp. 17-1–17-11.

Volpe, G.; and Melnik, R. E. 1985: A Method for Designing Closed Airfoils for Arbitrary Supercritical Speed Distributions. AIAA-85-5023.

Waggoner, Edgar G.; Campbell, Richard L.; and Phillips, Pamela S. 1985: Computational Wing Design in Support of an NLF Variable Sweep Transition Flight Experiment. AIAA-85-4074.

Wie, Y. S.; Collier, F. S., Jr.; and Wagner, R. D. 1991: *Application of Laminar Flow Control to High-Bypass-Ratio Turbofan Engine Nacelles.* SAE Tech. Paper Ser. 912114.